



Atmospheric and advective forcing of upwelling on South Africa's central Agulhas Bank

Lisa Hancke^{a,*}, David Smeed^b, Mike Roberts^{a,b}, Cristina Russo^c, Darren Rayner^b, Fatma Jebri^b

^a Nelson Mandela University, Gqeberha, South Africa

^b National Oceanography Centre, Southampton, United Kingdom

^c Oceans & Coasts Research Branch, Department of Forestry, Fisheries and the Environment, Cape Town, South Africa

ARTICLE INFO

Handling Editor: Prof. J. Aristegui

Keywords:

Agulhas Bank
Agulhas Current
upwelling
cold ridge

ABSTRACT

Current and temperature structures on South Africa's central Agulhas Bank are described from six months of moored observations and ancillary data collected during the seasonal transition from austral spring to summer (October 2018–March 2019). The occurrence of an intermittent mid-shelf upwelling ridge, associated with increased productivity, is an important part of the shelf's thermal structure. However, the subsurface evolution of this cold ridge has not been documented to date. A mooring array that transected the wide central shelf captured the seasonal increase in stratification that culminated in the formation of a cold ridge in late summer. We show that the cold ridge originates in the wind-driven upwelling zone on the eastern Agulhas Bank and emphasise the importance of oceanic forcing in maintaining the subsurface thermal structure through advective steering of wind-driven coastal upwelling plumes and through dynamic shelf edge upwelling. The main source of the cold basal layer at the mooring transect originated from upwelling further east, but persistent near-seabed temperatures $<9^{\circ}\text{C}$ on the outer shelf during the encroachment of the Agulhas Current confirm the contribution of shelf edge upwelling, offshore of the mooring transect, to the cold bottom layer on the Agulhas Bank. Of particular interest is the strengthening of the south-westward shelf current, inshore of cyclonic flow in the Agulhas Bight that accelerated the offshore advection of productive coastal water in the shape of the cold ridge. We show the shelf circulation to be highly coherent across and along the shelf. Shelf-wide barotropic pulses were driven by increased zonal wind stress that was in turn associated with variation in coastal sea level. In the light of global climate change, this work highlights the importance of long term in-situ monitoring in understanding ecosystem functioning on the highly dynamic Agulhas Bank.

1. Introduction

The Agulhas Bank (Fig. 1) is the broad, triangular shaped continental shelf at the southern tip of Africa. Its exposed, mid-latitude location between an eastern and western boundary current system, creates a unique and dynamic environment with relatively high year-round primary productivity (Mazwane et al., this issue) that supports a rich biodiversity and several endemic and commercially important fish stocks (Hutchings et al., 2002).

The Agulhas Bank can be divided into sub-regions according to the main forcing mechanisms that drive productivity on different parts the shelf. The cool western Agulhas Bank (18.5° – 20° E) is part of the Benguela Upwelling System (Shannon, 1985). Intensification of equatorward winds in austral spring and summer drives sustained seasonal

upwelling onto the western shelf. Net flow in the surface layer is equatorward and eastward movement of cold bottom water is restricted by the shallow bathymetry of the Alphonse Bank (Chapman and Largier, 1989) at 21° E. Oceanic forcing on the outer western Agulhas Bank is substantial (Largier et al., 1992) and warm Agulhas Current water is often observed flowing northwards along the western shelf edge (Lutjeharms et al., 2007; Lutjeharms and Cooper, 1996).

On the zonally orientated shelf, east of Cape Agulhas (20° E), upwelling is driven by a combination of atmospheric and oceanic processes. The separation of the warm and powerful Agulhas Current from the coast at Port Alfred (27° E) creates a divergent upwelling cell (Lutjeharms et al., 2000) where deep, dynamic upwelling is continuously maintained by the interaction of the Agulhas Current with the widening shelf. This is thought to be the main source of the cold basal layer that

* Corresponding author.

E-mail address: hancke.lisa@gmail.com (L. Hancke).

<https://doi.org/10.1016/j.dsr2.2023.105293>

Received 17 January 2022; Received in revised form 6 April 2023; Accepted 20 April 2023

Available online 24 April 2023

0967-0645/© 2023 The Authors. Published by Elsevier Ltd. This is an open access article under the CC BY license (<http://creativecommons.org/licenses/by/4.0/>).

spreads westwards over the Agulhas Bank (Largier and Swart, 1987; Lutjeharms, 2006). The strongest cooling events at Port Alfred are forced by a combination of Agulhas Current meanders and upwelling favourable winds (Leber et al., 2016). Under the right conditions cold water ($<17^{\circ}\text{C}$) can persist at the sea surface for several weeks and be advected westwards over the Agulhas Bank (Walker, 1986) and into adjacent bays (Beckley, 1988; Goschen and Schumann, 1988).

The outer parts of the eastern and central Agulhas Bank are dominated by the Agulhas Current that flows poleward along the south-eastern shelf edge. Currents on the outer shelf are strong and predominantly south-westward, turning south-southwest with the bathymetry of the Agulhas Bight ($22\text{--}23^{\circ}\text{E}$). Increased horizontal shear, caused by the transition to a wider shelf, creates instability in the southern Agulhas Current that leads to more sideways meandering (Goschen and Schumann, 1988; Lutjeharms, 1981). Shear-driven eddies on the shoreward border of the southern Agulhas Current have a substantial effect on the adjacent shelf water (Lutjeharms et al., 2003; Swart and Largier, 1987). These clockwise rotating, cold core eddies with diameters between 50 and 100 km, tend to concentrate in the eastward-facing Agulhas Bight where they can remain trapped (Lutjeharms et al., 1989). Their presence is associated with significant ($>1\text{ m s}^{-1}$) north-eastward reversals and upwelling above the shelf edge (Boyd et al., 1992). Meanders and eddies are usually trailed by plumes of warm Subtropical Surface Water that can disperse over large parts of the adjacent shelf (Goschen and Schumann, 1994).

As the shelf widens westward, the influence of the Agulhas Current on the inner shelf becomes less important. The Tsitsikamma coast, between Knysna and Cape St. Francis (Fig. 1) is known for intense coastal upwelling (Schumann, 1999; Schumann et al., 1982) driven by an increase in easterly winds in summer and autumn (Jury, 1994). The abrupt bathymetry of the straight, zonally orientated coastline allows cold bottom water, from upwelling further east, to be immediately accessible

close to the coast. Coastal upwelling thus progresses rapidly with the onset of easterly winds and provides a good indication of upwelling in the adjacent ocean (Schumann, 1999). The upwelling system here is distinctly different from that on the western Agulhas Bank due to more frequent alongshore fluctuations of the wind that often results in consecutive upwelling and downwelling cycles. On the south coast, upwelling occurs over typical periods of a day, with few events lasting longer than 4 days (Schumann, 1999). The relationship between the wind, currents and temperature variation along the Tsitsikamma coast is described by Hancke et al. (this issue).

An important feature of the central Agulhas Bank thermal structure is the seasonal (summer–autumn) occurrence of a mid-shelf upwelling ridge positioned roughly along the 100 m isobath (Fig. 1). This cold ridge originates in the coastal upwelling zone on the Tsitsikamma Coast and detaches from the coast further west. It is mostly identified from its surface signature in satellite remote sensing. It has been described as a quasi-permanent feature of the shelf thermal structure (Swart and Largier, 1987) characterised by a gentle doming of cool isotherms over the mid-shelf, where its presence is associated with increased productivity (Jacobs et al., this issue; Probyn et al., 1994; Verheye et al., 1994).

The connection between the cold ridge and wind-driven coastal upwelling was first established by Walker (1986) and later supported by Roberts (2005). Both authors used satellite observations to identify the cold ridge and found that a high occurrence of easterly wind resulted in the south-westward advection of coastal upwelling plumes from the Knysna–Tsitsikamma coast. Surface drifter trajectories (Hancke et al., this issue) confirm the connection of the cold ridge with wind-driven upwelling from the Tsitsikamma coast through south-westward flow along the 100 m isobath. Moreover, their work reveal the importance of oceanic forcing of the shelf current in cold ridge formation through increased south-westward advection of coastal upwelling plumes in the presence of Agulhas Current meanders.

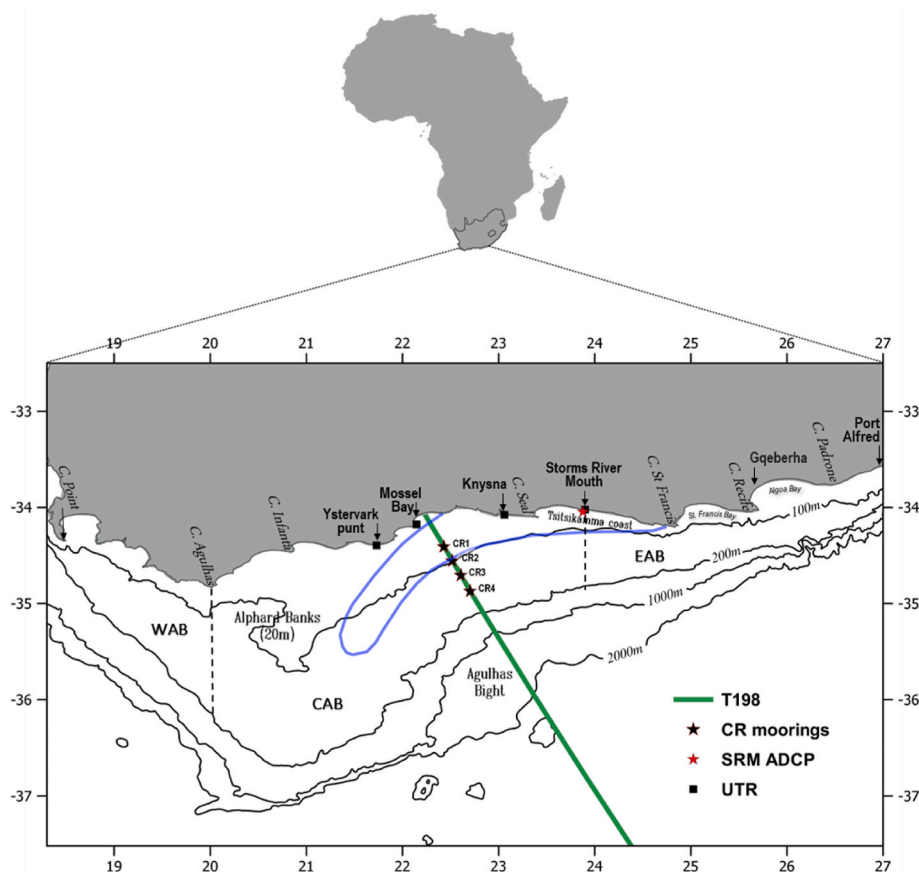


Fig. 1. Bathymetric map of the Agulhas Bank (AB) divided into western (WAB), central (CAB) and eastern regions (EAB). Four moorings (black stars), positioned 20 km apart along Jason altimeter track #198 (green line), measured current and temperature profiles associated with the cold ridge (blue outline), a mid-shelf upwelling plume. The red star shows the location of the Storm River Mouth (SRM) current profiler at $\sim 25\text{ m}$ water depth. Black squares show the location of underwater temperature recorders (UTRs) deployed near the coast at $\sim 12\text{ m}$ water depth.

Repeat in situ observations of the cold ridge over a six-month period (Swart and Largier, 1987) also suggest that the cold ridge is oceanically forced. The shoaling of isotherms inshore of western boundary currents systems are well documented, and work by Chang (2008) and Krug et al. (2014) highlights the importance of the Agulhas Current in priming the Agulhas Bank seabed with cold water along the south-eastern shelf edge. However, it is uncertain whether this geostrophic adjustment is sufficient to raise isotherms over the interior of the wider central shelf to form the cold ridge. Boyd and Shillington (1994) proposed that the cold ridge is forced by surface divergence related to the continuous widening of the shelf between Port Elizabeth and Knysna. They argued that the interaction of the Agulhas Current with the shelf edge alone cannot account for interior shelf upwelling that constitutes the cold ridge, and that an increase in divergence, driven by both the Agulhas Current (on the outer shelf) and by the wind (on the inner shelf), is required for cold ridge formation. Work by Lutjeharms et al. (1996) also links the cold ridge with the continuous lateral movement of cold bottom water along the 100 m isobath from its main source at the divergent Port Alfred upwelling cell.

Recent studies (Goschen et al., 2015; Leber et al., 2016; Leber and Beal, 2015; Malan et al., 2018; Pivan et al., 2016; Russo et al., 2019) have focussed on the influence of large solitary meanders in the Agulhas Current on the narrow eastern shelf. These Natal Pulses originate in the northern reaches of the Agulhas Current and can displace the Current core offshore by up to 200 km (Rouault and Penven, 2011). Previous authors agree that Natal Pulses facilitate the exchange of shelf and slope water and drive or enhance upwelling (and downwelling) on the narrow eastern shelf. Although analogous, this does not adequately address the role of smaller meanders that regularly form in the southern Agulhas Current, downstream of Port Elizabeth (now Gqeberha), on mid-shelf upwelling and cold ridge formation on the wide central shelf.

In this study we present six months of in situ current and temperature profiles collected at a mooring array that transects the central Agulhas Bank, offshore Mossel Bay, during the seasonal transition from austral spring to summer in 2018/2019. Together with ancillary data we explore the drivers of circulation and upwelling on the eastern and central Agulhas Bank, as well as the role of atmospheric and advective forcing in the formation and stability of the cold ridge.

2. Data and methods

2.1. In situ observations

The primary mooring dataset presented here was collected during the South African case study of SOLSTICE-WIO (<https://solstice-wio.org/>) — a multi-disciplinary project to investigate the environmental drivers and socio-economic consequences of the collapse of the chokka squid fishery on the Agulhas Bank. Four moorings were deployed offshore Mossel Bay between October 2018 and March 2019, along a transect that aligns with Jason/TP altimeter ground track #198 (Fig. 1). The transect crosses the wide central Agulhas Bank where the bathymetry slopes gradually to the shelf break (200 m isobath) located approximately 130 km from the coast. Seawards of the shelf break, where the Agulhas Current is found, the 1000–2000 m isobaths create a large eastward facing embayment, subsequently referred to as the Agulhas Bight.

Four moorings were spaced 20 km apart along the cold ridge (CR) mooring transect, with the inshore mooring (CR1) positioned 40 km from the coast and the offshore mooring (CR4), 30 km from the shelf break. Mooring placement was selected to avoid the nearshore fishing grounds, while intersecting the subsurface current and temperature structure associated with the cold ridge. Alignment with altimeter track #198 also provides the opportunity for the comparison of in situ velocities with altimeter derived geostrophic velocities.

Each CR mooring recorded velocity profiles in 4 m vertical bins at 10-min intervals with an upward-looking Nortek Signature 250 kHz

Acoustic Doppler Current Profiler (ADCP) mounted 3 m above the seabed. Ensembles were averaged for 2 min using 58 water pings, giving a horizontal velocity precision of 0.57 cm s^{-1} . ADCP earth coordinates were corrected for magnetic declination (28°W) and transformed to a coordinate system where the u and v components represent velocities across and along the mooring transect respectively. These are equivalent to along-shelf (u) and cross-shelf velocities (v). Velocity data were flagged for outliers, repeat values and sidelobe interference which typically eliminates the top 10% of the water column. A thermistor string of Star-Oddi underwater temperature recorders (UTRs) measured water column temperature at 10-min intervals with a vertical spacing of 7 m ($<60 \text{ m}$ depth) or 15 m ($>60 \text{ m}$ depth) at each CR mooring. Pressure sensors on the surface and bottom flotation monitored mooring subduction during strong current events. The temperature profiles were corrected for variations in water depth using the method described in Appendix A (supplementary material) and then interpolated onto a grid with 4 m vertical spacing to match the vertical resolution of the ADCP data.

A second ADCP was deployed 160 km east of the CR transect, at Storms River Mouth (SRM), off the Tsitsikamma coast, for the duration of the CR mooring deployment. This Nortek AWAC 600 kHz ADCP, deployed in the nearshore at a depth of 27 m, was configured to record hourly velocity profiles in 2 m vertical bins with a horizontal velocity precision of 2.2 cm s^{-1} , as well as bottom temperature. ADCP earth coordinates were corrected for magnetic declination (28°W) and the quality-controlled velocity data were transformed to a coordinate system where the dominant u-component aligns with the Tsitsikamma coastline and the v-component represent cross-shore velocity. Data from the SRM ADCP is limited to between 26 October 2018 and 21 January 2019 due to premature instrument failure.

Other in situ data used in the analysis are hourly records of coastal seawater temperature at $\sim 12 \text{ m}$ depth from UTR stations at Storms River Mouth, Knysna, Mossel Bay and Ystervarkpunt, provided by South Africa's Department of Forestry Fisheries and Environment (DFFE); and hourly sea level records from a tide gauge at Mossel Bay provided by the South African Hydrographic Office (SANHO). The sea level data was corrected for the inverse barometer effect using hourly records of atmospheric pressure from a nearby automatic weather station maintained by South African Weather Services (SAWS). The resultant adjusted sea level used throughout this paper is therefore a combination of the measured sea level (referenced to lowest astronomical tide) at Mossel Bay and the variation in measured air pressure from the mean atmospheric pressure (1013 mb).

All in situ data were low-pass filtered using a Tukey window with a 36-h cut-off period to remove high frequency processes such as tides and inertial oscillations ($\sim 21 \text{ hr}^{-1}$). Deployment details and the profiling

Table 1

Deployment information and profiling ranges of the moored data. Velocity and temperature profiles were recorded at 10-min intervals at the cold ridge mooring transect (CR1–CR4). Current profiles and bottom temperature were recorded hourly at the Storms River Mouth ADCP and the coastal UTRs measured hourly coastal temperature at Storms River Mouth (SRM), Knysna (KY), Mossel Bay (MB) and Ystervarkpunt (YP).

Morning ID	Lat ($^\circ \text{S}$)	Lon ($^\circ \text{E}$)	Water depth (m)	Depth range velocity profiles (m)	Depth range temperature profiles (m)
CR1	34.408	22.429	87	17–81	23–80
CR2	34.556	22.517	102	16–96	17–90
CR3	34.706	22.607	115	17–109	16–103
CR4	34.870	22.704	131	15–123	20–121
SRM	34.045	23.877	27	5–25	25
ADCP					
SRM UTR	34.023	23.900	12	n/a	n/a
KY UTR	34.076	23.060	12	n/a	n/a
MB UTR	34.177	23.146	12	n/a	n/a
YP UTR	34.395	23.731	12	n/a	n/a

ranges after quality control procedures are given in Table 1.

2.2. Wind data

ERA-5 reanalysis data of zonal and meridional winds at 25 km spatial resolution, produced by the European Centre for Medium-Range Weather Forecasts (ECMWF), at a standard height of 10 m above sea level at the CR mooring transect were downloaded from the Copernicus Climate Change Service (C3S) (<https://cds.climate.copernicus.eu>; Hersbach et al., 2019). Hourly data at the mooring transect were low-pass filtered and interpolated to 10-min intervals to match the temporal resolution of the moored measurements. Coordinates were transformed to align with the CR mooring transect, so that the u and v velocities represent across-track (x) and along-track (y) winds respectively. Wind stress components (τ_x ; τ_y) were calculated from the square of the wind speed at 10 m above the sea following (Kara et al., 2007).

2.3. Satellite data

2.3.1. Altimetry

Information on the strength and position of the Agulhas Current relative to the shelf edge was extracted from delayed-time, gridded satellite altimetry using the LACCE (Location of the Agulhas Current's Core an Edges) algorithm (Russo et al., 2021). The algorithm defines the Agulhas Current core as the location of the local maximum current speed and the Agulhas Current edges as the location of the local maximum gradient in current speed. Data were extracted along satellite altimeter Jason 3 track #198 to determine daily variations in the distance of the shoreward edge of the Agulhas Current from the shelf break (200 m isobath), offshore of the mooring transect. The $0.25^\circ \times 0.25^\circ$ gridded altimetry product is processed by CLS (previously by AVISO (Archiving, Validation and Interpretation of Satellite Oceanographic Data) and distributed by CMEMS (<https://marine.copernicus.eu/services-portfolio/access-to-products/>) as a level 4 multi-mission product, consisting of daily, gridded Sea Level Anomaly (SLA) and derived variables computed with respect to a twenty-year mean (Rio et al., 2014).

Current shear was calculated using geostrophic current speed from the same gridded altimetry dataset. Shear at the shelf edge, offshore of the mooring transect, was calculated using the intersection of track #198 and the difference in current speed at the two grid points adjacent of the 200 m isobath.

2.3.2. Sea surface temperature (SST)

Daily Multiscale Ultrahigh Resolution (MUR) Level 4 SST (MUR-JPL-L4-GLOB-v4) provided by NASA's Jet Propulsion Laboratory (JPL) was downloaded from <https://podaac-tools.jpl.nasa.gov/las>. The 0.01° (1 km) spatial resolution data was used to detect upwelling at the ocean surface and to monitor the position and behaviour of the Agulhas Current along the south-eastern shelf edge of the Agulhas Bank.

2.3.3. High frequency (HF) radar

Three WERA (WavE RADar) HF Ocean Radar stations, manufactured by Helzel Messtechnik GmbH, were installed by ACTIMAR and CLS Southern Africa on the south coast of South Africa to monitor variability in the Agulhas Current during offshore exploration activities. The radial velocities, estimated by the conventional beam-forming method, were combined on a Cartesian grid at 6 km resolution and made available every 30 min. For details and potential of the WERA HF Radar technology for ocean application see (Helzel et al., 2009).

2.4. Data analysis

2.4.1. Variance ellipses

Variance ellipses of filtered ADCP velocities were computed using the Matlab toolbox, jLab (Lilly, 2021). The resultant co-variance matrix gives the spread of the data in both the along-shelf (u) and cross-shelf (v)

components. Ellipse size (k) is the root-mean-square of the semi-major and semi-minor axes. Ellipse shape (λ) is the ratio between the minor axis and the major axis with values closer to 1 showing greater polarisation in the flow. To enable direct comparison of variance ellipses and time-mean vectors on the central and eastern shelf (Fig. 2) only data that correspond to both the CR and SRM deployments were used in these analyses.

2.4.2. Singular value decomposition (SVD)

Filtered ADCP velocities were reduced to their dominant modes of variability through SVD. The method uses the detrended u and v velocities simultaneously to identify patterns that are coupled in both components. Each pair of orthogonal modes thus represents the percentage of the squared co-variance between the two velocity components. Time-series of the dominant modes, hereafter referred to as expansion coefficients (ECs), were calculated by projecting the dominant singular vectors onto the corresponding velocity component timeseries.

Time-lagged correlations were performed between the ECs of the dominant SVD modes at each CR mooring and the following independent variables: (1) wind stress (τ_x τ_y) at the CR mooring transect, (2) coastal sea level at Mossel Bay, (3) the LACCE distance of the shoreward edge of the Agulhas Current from the shelf break at track #198 and (4) altimeter derived surface current shear at the shelf edge along track #198.

3. Results

3.1. Shelf currents

3.1.1. Variance ellipses and mean flow

Variance ellipses and time-mean velocity vectors of the ADCP measured currents are given in Fig. 2. At the CR transect, the major axes of the surface co-variance were generally aligned northeast-southwest (NE-SW) with the mid-shelf bathymetry. Ellipse orientation rotated clockwise with depth at all CR locations, resulting in the east-west alignment of bottom ellipses. The clockwise rotation through the water column increased with distance offshore to 45° at CR4. Polarisation increased with depth and closer to shore, with surface currents

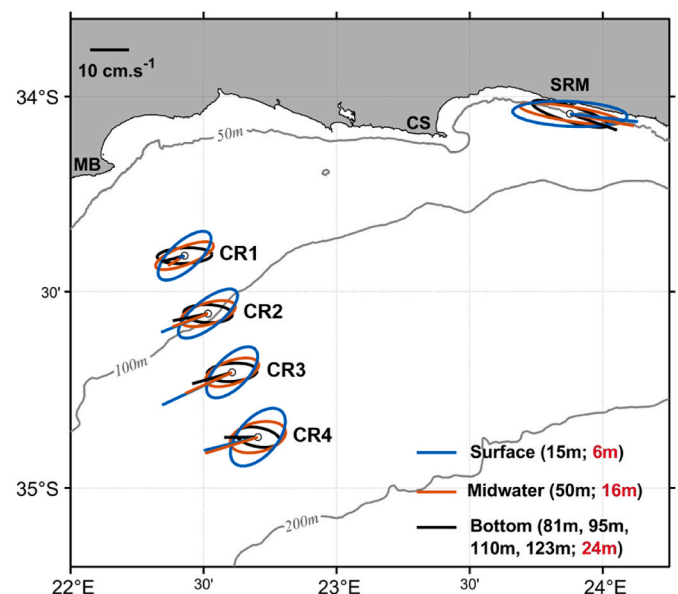


Fig. 2. Velocity variance ellipses and time-mean vectors for three depths at each mooring location. Abbreviated place names are Mossel Bay (MB), Cape Seal (CS) and Storms River Mouth (SRM). Measurement depths at the SRM ADCP are shown in red.

on the outer shelf (CR4) being most isotropic and the flow at CR1, specifically near the bottom, most directionally aligned in an NE-SW direction. At SRM the flow at all depths was strongly aligned with the coastal bathymetry. Ellipse size at SRM decreased more markedly with depth, but the clockwise rotation between the surface and bottom ellipse orientation was only 12°. Compared to the CR transect, variance ellipses at SRM were larger and more polarised, highlighting strong directional flow aligned with the Tsitsikamma coast.

Time-mean velocity vectors (Fig. 2) show the dominance of SW flow at the CR mooring transect. A mean flow of 20 cm s⁻¹ was recorded near the surface at CR3, while mean flow on the outer shelf (CR4) reached 14 cm s⁻¹ at the surface (15 m) and midwater (50 m). Weak mean flow at CR1 (surface = 2 cm s⁻¹; bottom = 6 cm s⁻¹) points to more variable flow direction on the inner part of the central shelf. In contrast, the mean flow at SRM was directed eastwards at all depths, with mean surface and bottom velocities of 18 cm s⁻¹ and 13 cm s⁻¹ respectively. At all sites the mean directional flow in the upper water column (<50 m depth) was closely aligned, while bottom mean flow rotated clockwise with respect

to the surface. The angle of the clockwise rotation increased with distance offshore, resulting in a mean westward bottom flow of 8.5 cm s⁻¹ at CR4.

3.1.2. Velocity components (SRM vs CR transect)

The shelf circulation is further examined through contour plots of the ADCP measured u and v velocity components in Figs. 3 and 4 respectively. An important observation is the strong correlation between zonal wind stress and coastal sea level variation that, in turn, correspond to variability in the shelf flow. In addition, these data highlight differences and similarities in the velocity structures at SRM and the CR transect.

Along-shelf flow at SRM (Fig. 3b) was strong (max = 84 cm s⁻¹) and predominantly eastward (80%). At SRM, barotropic eastward pulses with depth-mean velocities >30 cm s⁻¹ were sustained for up to 4 days and had an occurrence of 24%. These strong eastward currents were interrupted by periods of weaker westward flow (depth-mean <10 cm s⁻¹) associated with a change to easterly wind and lower sea level. In contrast, along-shelf flow at the CR transect (Fig. 3 c-f) was

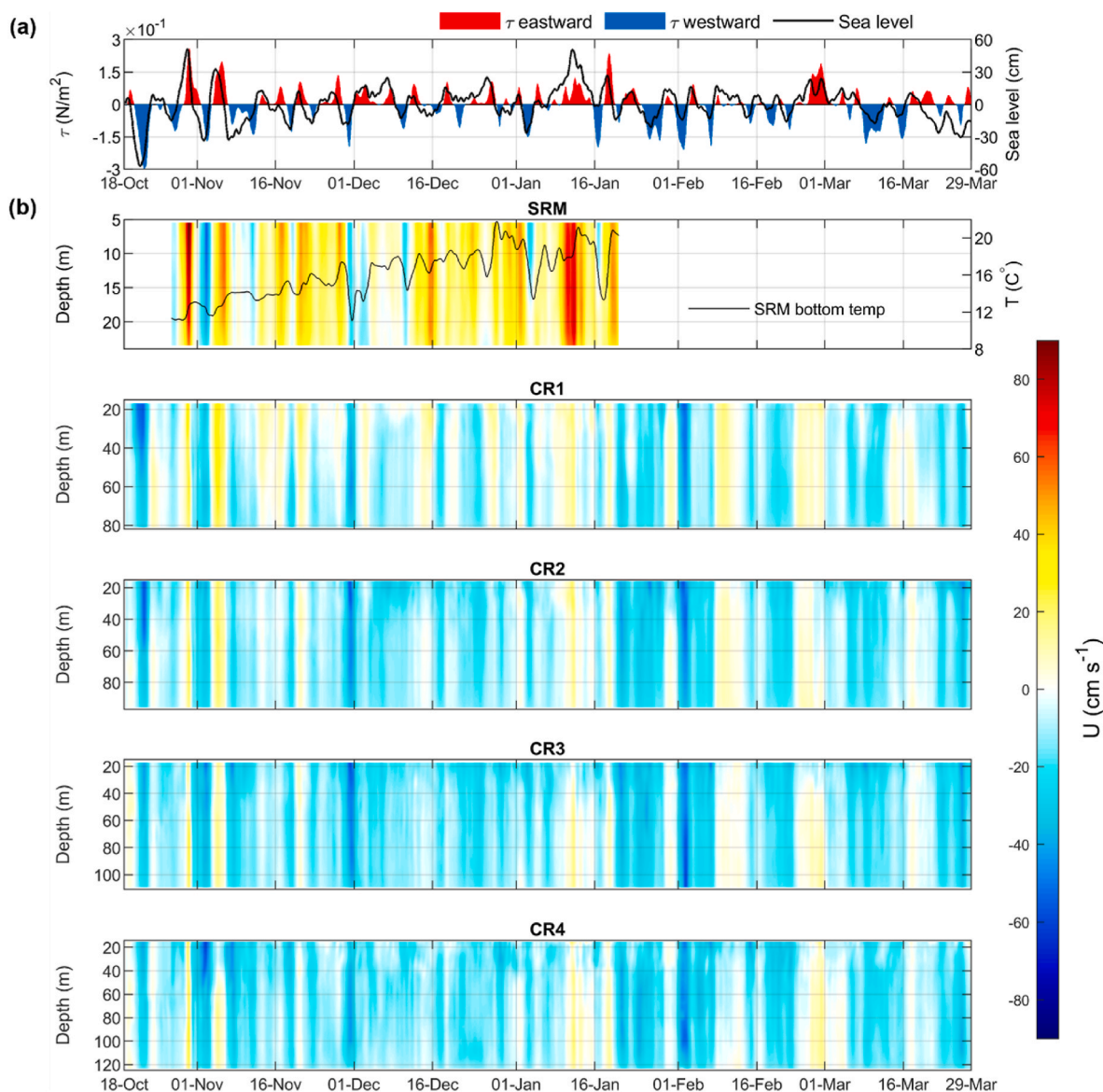


Fig. 3. (a) Left axis – Zonal wind stress (τ_u) at the mooring transect. Positive (red) and negative (blue) values denote westerly (downwelling) and easterly (upwelling) winds respectively. Right axis - normalised sea level (black line) at Mossel Bay. (b) Depth-time contours of the along-shelf (u) velocity at each mooring. Positive (yellow-red) and negative (blue) values denote north-eastward and south-westward flow respectively. For Storms River Mouth (SRM) corresponding temperature at 25 m is shown by the black line.

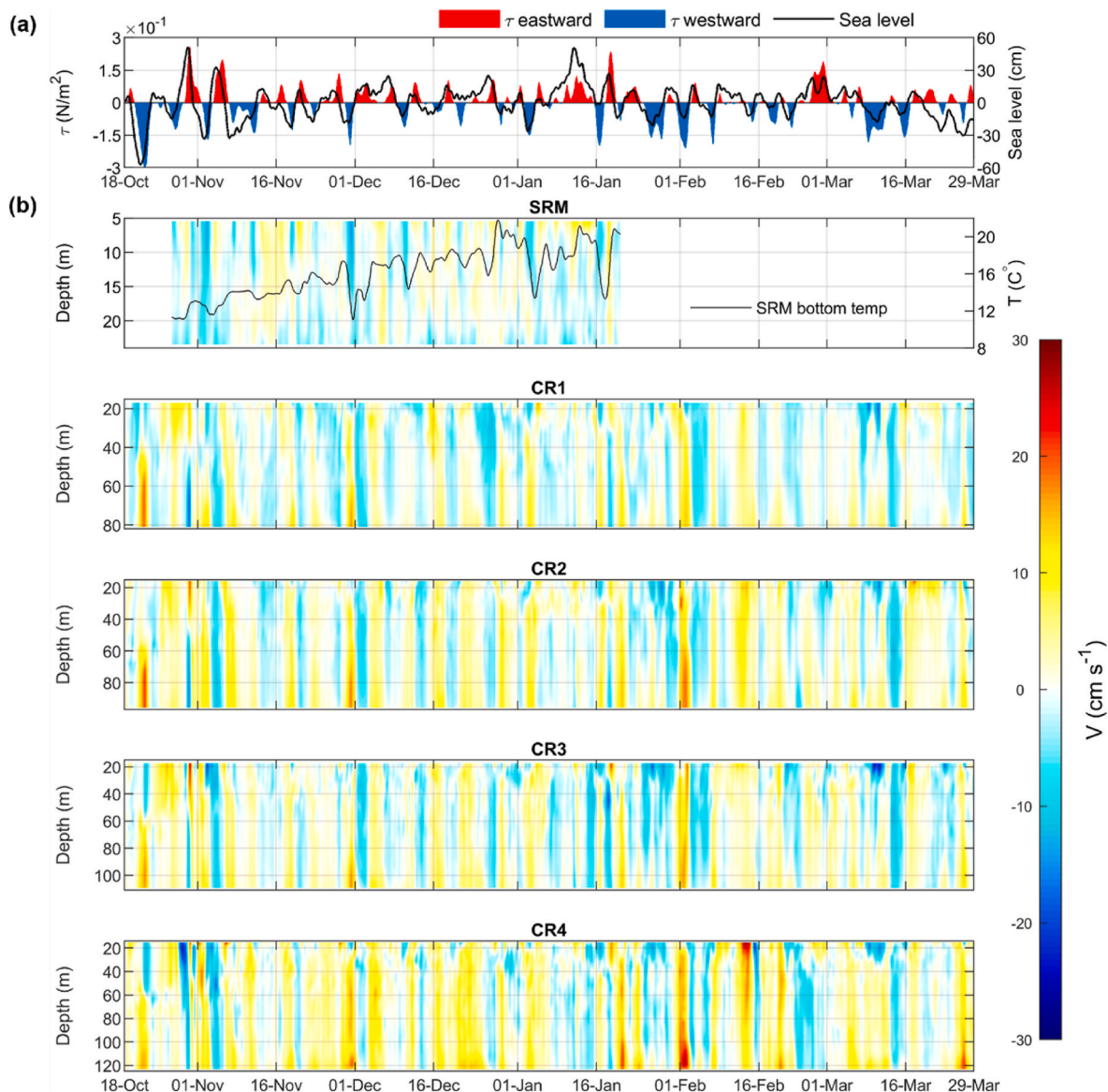


Fig. 4. (a) Left axis – Zonal wind stress (τ_u) at the mooring transect. Positive (red) and negative (blue) values denote westerly (downwelling) and easterly (upwelling) winds respectively. Right axis - normalised sea level (black line) at Mossel Bay. (b) Depth-time contours of the cross-shelf (v) velocity at each mooring. Positive (yellow–red) and negative (blue) values denote onshore and offshore flow respectively. For Storms River Mouth (SRM) corresponding temperature at 25 m is shown by the black line (right axis).

predominantly SW and weaker. The occurrence of SW flow increased with distance offshore, from 72% at CR1 to 91% at CR4. Depth-averaged SW velocities $>30 \text{ cm s}^{-1}$ were sustained for up to 2 days, but made up $<7\%$ of the total alongshore flow at the CR transect. Strong SW pulses ($>50 \text{ cm s}^{-1}$) always occurred during peak easterly wind stress. During these strong current episodes the SW surface maximum could be found on the inner shelf (20–22 October), outer shelf (31 October–2 November) or on the mid-shelf (29 November –1 December; 1–3 February).

Compared to the along-shelf (u) component, cross-shelf (v) currents (Fig. 4 b-f) were weak and more variable. Velocities $>10 \text{ cm s}^{-1}$ only contributed 1% of the total v -component at SRM, increasing to 5% at the CR transect. At SRM the dominance of onshore flow near the surface (64%) and offshore flow near the seabed (76%) indicates downwelling conditions during the measurement period at the Tsitsikamma coast (November 2018 to January 2019). At the CR transect the depth averaged cross-shelf flow was predominantly onshore, except at CR1 where onshore and offshore flow were nearly equally divided. Maximum

onshore surface velocities of $\sim 30 \text{ cm s}^{-1}$ were recorded at CR3 and CR4; and maximum onshore bottom velocities of $\sim 20 \text{ cm s}^{-1}$ at CR2, CR3 and CR4.

3.1.3. Barotropic structure and alongshore reversals

Despite the above-mentioned differences between ADCP measured currents at the CR transect and at SRM, velocity structures at all moorings were typically barotropic with a high level of coherence between sites. Depth averaged velocities between all sites were significantly correlated ($\alpha < 0.01$). The strongest zero-lag correlations were found between the u ($r > 0.9$) and v ($r > 0.8$) components of adjacent CR moorings. However, strong correlations ($r > 0.7$) at lags of 6–8 h were also found between the alongshore flow at all CR moorings and the alongshore flow at SRM, with flow at the CR transect leading that at SRM (For example, see CR2 and SRM in Fig. 5.).

SVD of the moored current profiles (Fig. 6) confirm the dominance of the barotropic u -component and baroclinic v -component at all sites. The dominant 1st mode accounts for $>90\%$ of the variance at all stations.

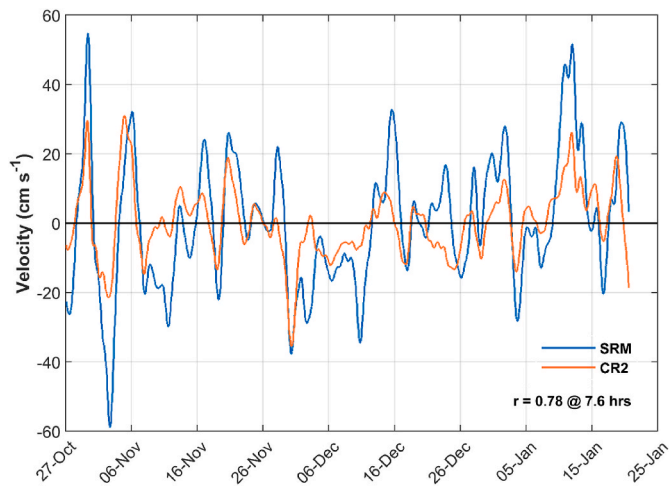


Fig. 5. Time series of the normalised, depth-averaged along-shelf (u) velocity at the Storms River Mouth (SRM) and CR2 moorings. Positive and negative values denote north-eastward and south-westward flow respectively. Time-lagged Pearson’s correlation coefficient (r) is significant at $\alpha = 0.01$.

The magnitude of the 1st mode u-component is almost constant with depth. The magnitude of the 1st mode v-component changes signs at 20–30 m below the surface and is bottom intensified at all stations, except at SRM where the surface magnitude is greater. The 2nd mode (not shown) accounts for only 5% of the total variance at CR4, decreasing to < 2% for all other stations.

Singular modes produced by SVD are data modes that don’t represent actual physical processes. To put the results into perspective we associate the dominant singular modes of velocity at the CR transect with physical forcing through time-lagged correlations of their expansion coefficients (ECs) with several independent variables that represent atmospheric and advective forcing. Correlation time series are normalised daily averages and time lags were limited to 10 days. Reported r values are significant at $\alpha < 0.01$.

Moderate zero (day) lag correlations were found between the 1st mode u-component ECs at all CR moorings and (1) coastal sea level

variation ($r = 0.54$ – 0.59), and (2) along-shelf wind stress ($r = 0.46$ – 0.53). The 1st mode v-component ECs at CR1 and CR2 also had moderate zero (day) lag correlation with the cross-shelf winds stress ($r = 0.59$ and $r = 0.51$ respectively) and with coastal sea level ($r = 0.51$ and $r = 0.48$ respectively). Weaker correlations were also found between the 2nd mode EC (u-component) at CR4 and (1) the LACCE distance of the shoreward border of the Agulhas Current from the shelf break ($r = 0.47$ at lag -9 days), and (2) geostrophic shear at the shelf break ($r = 0.41$ at lag -9 days).

The response of the water column to increasing percentiles of wind stress is summarised in Figs. 7 and 8 for easterly and westerly winds respectively. Because of their close association, wind stress is considered a proxy for sea level variation. The velocity structures for wind stress values below the 50th percentile were similar regardless of wind direction (compare Figs. 7a and 8a). Weak SW flow was dominant across the CR transect with weak onshore flow present along the transect. SW flow strengthened with easterly winds, reaching maximum velocities over the mid-shelf during peak easterly wind stress (Figs. 7c and 95th percentile). Offshore surface and onshore bottom Ekman flows strengthened with increasing percentiles of easterly wind stress. Similarly, the nearshore current turned NE with strengthening westerly winds, (Fig. 8b), but shelf-wide NE reversals were only associated with the strongest westerly winds (Fig. 8c; 95th percentile). At the same time, onshore surface an offshore bottom Ekman transport, indicative of downwelling, increased as westerly winds strengthened.

These results show that circulation on the Agulhas Bank is strongly influenced by alongshore wind stress that is, in turn, coupled with transient variations in coastal sea level. The correlation between the two variables suggests that they work in sympathy to drive strong SW barotropic pulses during easterly wind stress and lower sea level, and conversely, barotropic NE reversals during westerly wind stress and elevated sea levels. ADCP measurements show that both SW and NE pulses in the current can extend to the outer shelf on the wide central Agulhas Bank.

3.2. Shelf temperature and thermocline control

The thermistor string data collected at the CR mooring transect (Fig. 9) show progressive changes in the water column that reflect the

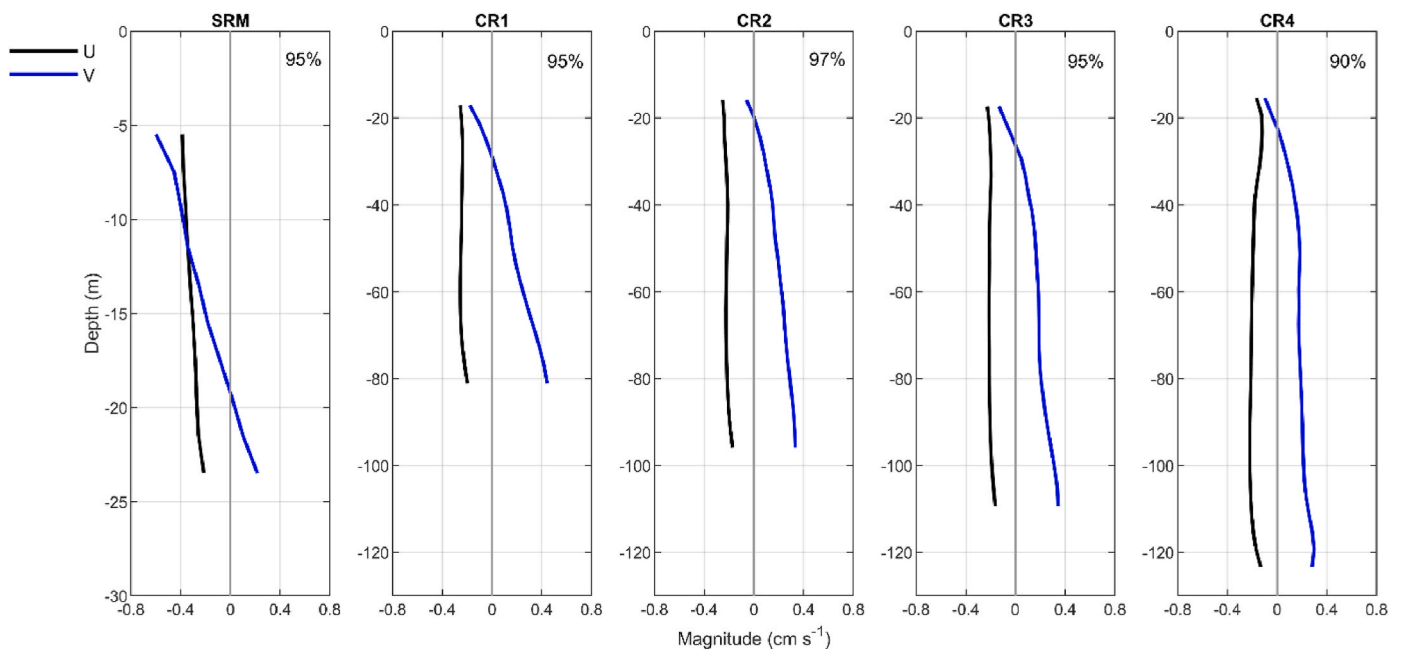


Fig. 6. Vertical profiles of the u (black) and v (blue) components of the 1st singular mode and its percentage contribution to the variance at each mooring. Note the different depth scale for Storms River Mouth (SRM) and all cold ridge (CR) moorings.

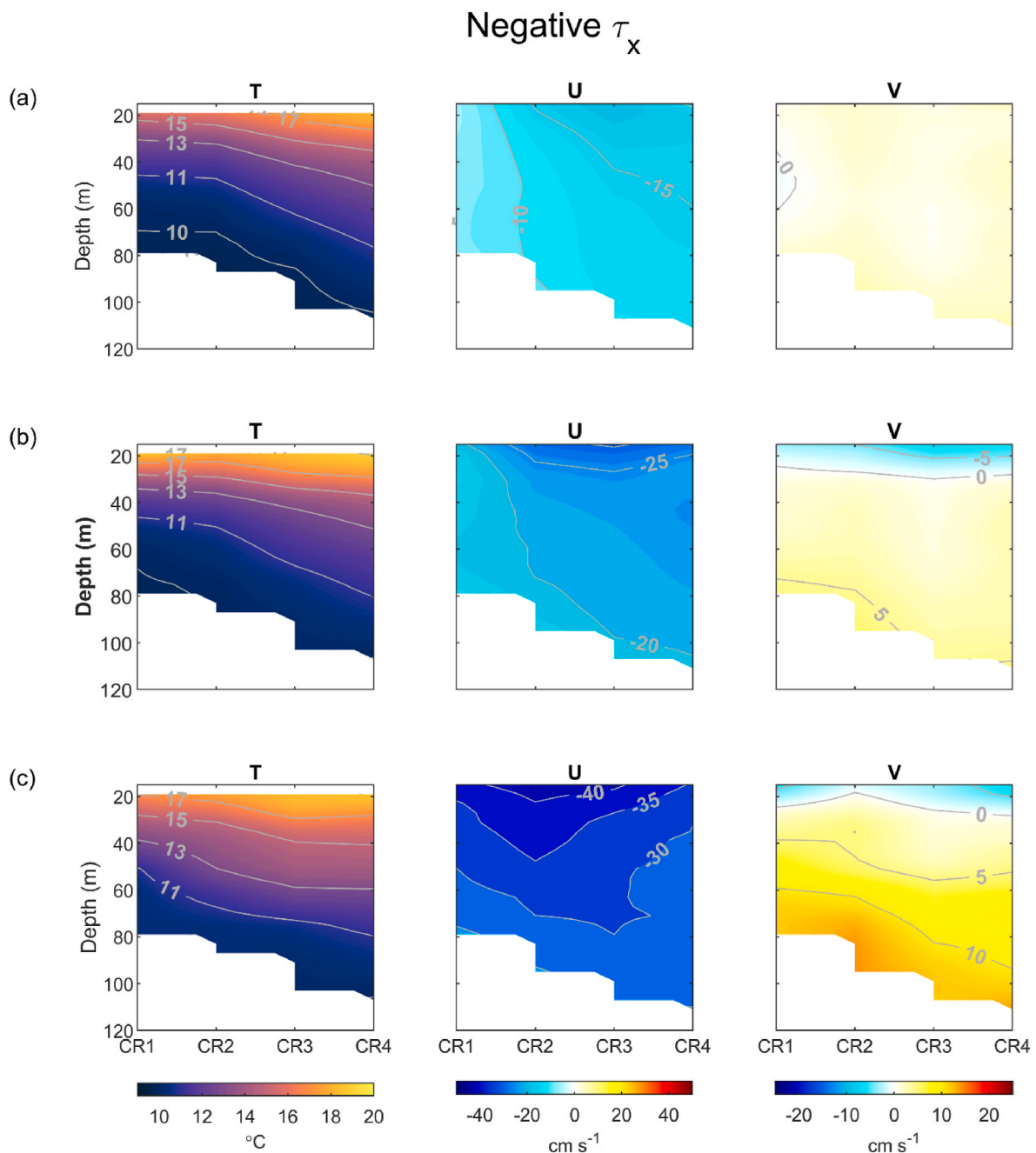


Fig. 7. Cross-isobath sections of temperature (T), along-shelf velocity (U) and across-shelf velocity (V) at the mooring transect, during increasing percentiles of easterly wind stress. T, U and V are temporally averaged for easterly wind stress (a) < the 50th percentile (b) > 50th and < 75th percentile and (c) > the 95th percentile.

seasonal transition from austral spring to summer. In October and November, the water column was cool and relatively weakly stratified. The strengthening of the cold bottom layer (<10 °C) together with surface warming in January resulted in highly stratified conditions, followed by extensive upwelling in February and March. Near-surface temperatures at the mooring transect ranged between 10 and 22 °C, with the warmest surface conditions on the mid-shelf during the second half of January and the coldest at CR1 during the upwelling event in February. Bottom temperatures <9 °C were recorded at all stations except CR1, with continuous records at CR3 and CR4 from 26 November to 27 December. The seabed temperature at the SRM ADCP ranged between 9 and 22 °C (Fig. 3) where a general warming trend was interrupted by brief upwelling episodes during peak easterly winds in December and January.

At the CR transect, large fluctuations (20–40 m) in the depth of the 14 °C isotherm (Fig. 9), typically over periods of two to four days, occurred during or after strong winds. For example, in October the depth of the 14 °C isotherm decreased by between 30 m (CR1 and CR4) and 40 m (CR2 and C3) during strong (50–80 km/h) and sustained easterly winds. A period of storm strength, zonally alternating winds at the end of October/start of November, accompanied by coastal sea level changes of up to 1 m, resulted in consecutive upwelling and downwelling cycles that were most pronounced in the nearshore (CR1). Extensive upwelling at the end of January and in February coincided with a period of predominantly easterly wind stress. However, on several occasions comparable winds stress did not produce the temperature responses at the CR transect described above. For example, we noted no upwelling during strong easterlies on 16 January, downwelling during strong easterlies

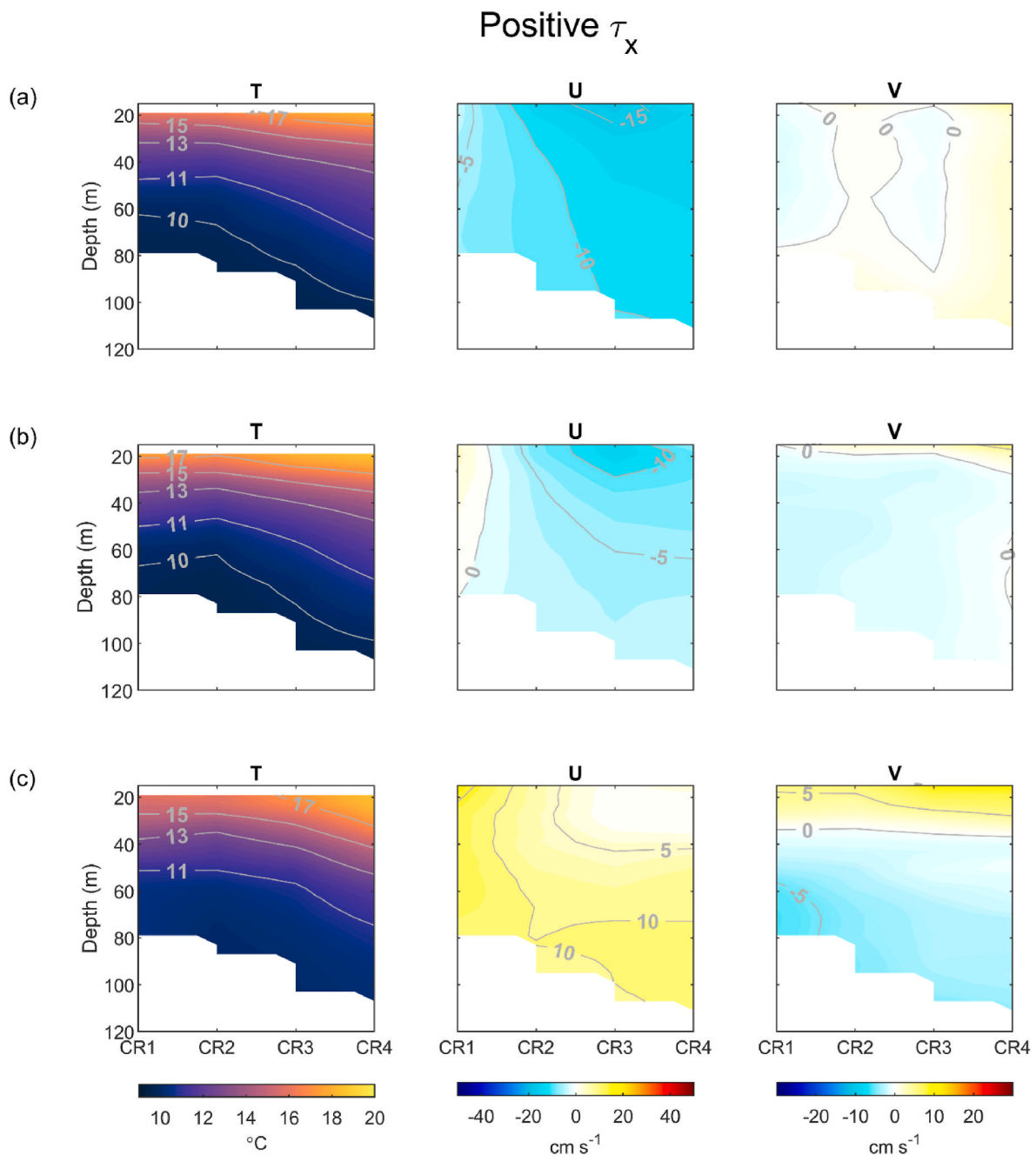


Fig. 8. Cross-isobath sections of temperature (T), along-shelf velocity (U) and across-shelf velocity (V) at the mooring transect, during increasing percentiles of westerly wind stress. T, U and V are temporally averaged for westerly wind stress (a) < the 50th percentile (b) > 50th and < 75th percentile and (c) > the 95th percentile.

winds from 9 to 12 March and surface cooling during light easterlies at the end of March.

The effect of increasing wind stress on the temperature structure at the mooring transect is summarised in the cross-shelf sections in Figs. 7 and 8 for increasing percentiles of easterly and westerly winds respectively. Of interest is the warming of the surface layer and increased stratification with strengthening upwelling favourable easterly wind. These conditions were accompanied by a strong SW shelf current (u), and offshore surface and onshore bottom flows (v). This warming of the surface layer ahead of the coastal upwelling front was also observed on the central Agulhas Bank during strong easterly winds by Schumann and van Heerden (1988). This is in direct contrast with the rapid onset of wind-driven upwelling along the Tsitsikamma coast.

The coolest depth averaged temperatures and greatest doming of

isotherms over the mid-shelf — conditions typically linked to the presence of the cold ridge — coincided with increasing percentiles of westerly wind stress (Fig. 8b and c). These conditions were accompanied by NE current reversals and downwelling conditions that accentuated the doming effect of isotherms over the mid-shelf at the mooring transect.

3.2.1. Advective vs atmospheric control of the shelf thermocline

The concept of advective control of the thermocline on the eastern Agulhas Bank was first proposed by Swart and Largier (1987). They suggested that intense stratification on the central and eastern Agulhas Bank in summer is a result of the vertical juxtaposition of warm, Sub-tropical Surface water (from Agulhas Current surface plumes) and cold, Indian Ocean Central water (upwelled along the south-eastern shelf

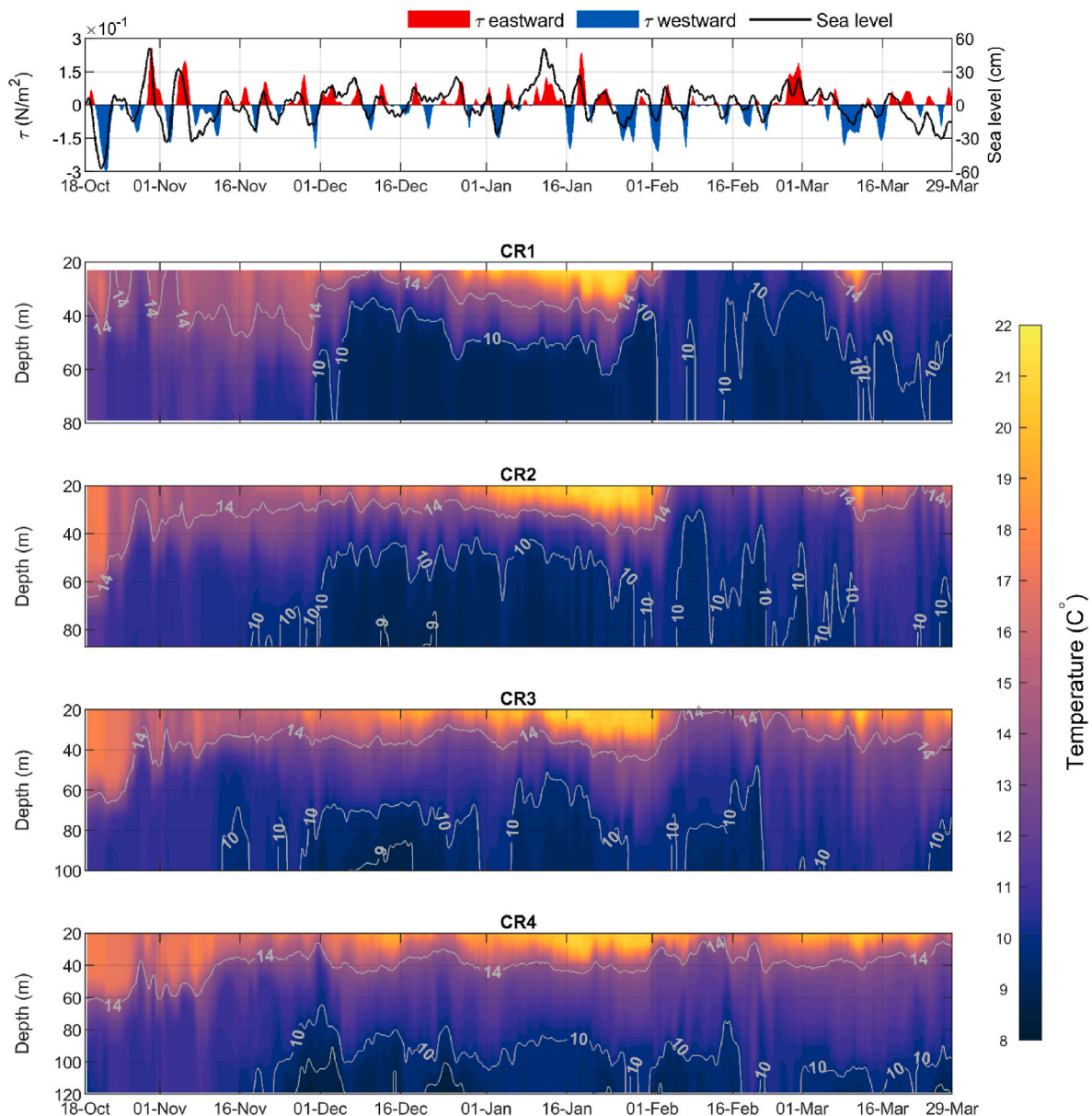


Fig. 9. (a) Left axis – Zonal wind stress (τ_w) at the mooring transect. Positive (red) and negative (blue) values denote westerly (downwelling) and easterly (upwelling) winds respectively. Right axis - normalised sea level (black line) at Mossel Bay. (b) Depth-time contours of temperature profiles for each mooring at the CR transect. The 10 $^{\circ}\text{C}$ and 14 $^{\circ}\text{C}$ isotherms represent the cold bottom layer and middle of the thermocline respectively. Water $<9^{\circ}\text{C}$ is indicative of South Indian Central Water upwelled from beyond the shelf break.

edge). Both processes are driven continuously by the interaction of the Agulhas Current with the bathymetry of the south-eastern shelf edge. However, a reduction in vertical, storm-induced mixing as well as increased solar heating in summer results in intense seasonal stratification on the shelf.

Hovmöller diagrams of daily average temperature at the mooring transect (Supplementary material S1) show simultaneous surface warming and bottom cooling that resulted in a highly stratified water column in January (days 80–103 of the mooring deployment). Satellite SST images (not shown) identify the source of the warm shelf water as (1) plumes from northward flows of the Agulhas Current along the western shelf edge and, to a lesser extent (2) surface plumes from Agulhas Current meanders along the south-eastern shelf edge that dispersed over large parts of the bank in December and January. The surface warming trend is also evident in the UTR data (Supplementary material S2a), with coastal temperature peaking at 24 $^{\circ}\text{C}$ in late January. At the same time bottom temperature at the mooring transect showed a

cooling trend, together with a general increase in the thickness of the cold bottom layer across the mooring transect.

The dynamics of shelf thermocline control is further investigated through a series of time-lag correlations between the area under selected isotherms at the mooring transect and atmospheric and advective forcing. Atmospheric forcing is represented by (a) daily mean zonal wind stress (τ_x) at the mooring transect and (b) coastal sea level at Mossel Bay. Advective forcing is represented by (c) the LACCE distance of the shoreward border of the Agulhas Current from the 200 m isobath along altimeter track #198 and (d) the geostrophic current shear at the intersection of altimeter track #198 and the 200 m isobath. For (c) and (d) the effective number of degrees of freedom was reduced by a factor of 7 to account for the coarse temporal resolution of the gridded AVISO altimetry product.

The area under the 9 $^{\circ}\text{C}$, 10 $^{\circ}\text{C}$ and 14 $^{\circ}\text{C}$ isotherms were chosen to represent newly upwelled Indian Ocean Central water, the established cold basal layer and the centre of the thermocline (Roberts, 2005)

respectively. Time series of the correlation variables during the mooring deployment period (Fig. 10) show the lateral displacement of the shoreward border of the Agulhas Current, in the order of 60 km, associated with meandering. Positive shear increased as the Current encroached on the shelf in December and March and periods of negative shear in November and February (when the Current was furthest offshore) represents cyclonic flow between the shelf edge and the shoreward border of the Agulhas Current.

Results from the lag correlation analysis (Fig. 11) show significant ($\alpha < 0.05$) positive (upwelling) and negative (downwelling) correlation with the proximity of the Agulhas Current and with the current shear at the shelf edge. Upwelling occurred before the Agulhas Current moved offshore (leading edge of meander) and after an increase in shear (shelf intrusion). Downwelling occurred after the Agulhas Current moved offshore (trailing edge of meander) and before an increase in shear (shelf intrusion). Upwelling and downwelling lag times in the cooler layers (9 °C and 10 °C) show significant correlation with the behaviour of the Agulhas Current at lags periods between 4 and 50 days (with peaks at 25 days), while the surface thermocline (14 °C isotherm) responded at shorter lag times of between 0 and 6 days.

Significant but weaker correlations were also found between changes in the isotherm areas and the atmospheric variables. For the 9 °C and 10 °C isotherms, upwelling occurred 0–4 days before and after an increase in coastal sea level, or the peak of a passing CTW. Downwelling occurred 0–4 days before and after a decrease in coastal sea level (or the trough of a passing CTW). Correlation of the surface thermocline (14 °C) and coastal sea level show the same pattern, but at lags of 0–1 day. Only the area under surface thermocline was significant (and positively) correlated with alongshore wind stress. Upwelling (downwelling) occurred 2–3 days before increasing westerly (easterly) winds. This result can be explained by the strong zonally alternating nature of wind stress on the Agulhas Bank, where sequential upwelling and downwelling cycles are regularly observed.

3.3. Case study – cold ridge formation during wind-driven upwelling and an Agulhas Bight cyclone

Extensive coastal upwelling at the end of January and the formation of the cold ridge in February is associated with the increase in the strength and occurrence of easterly winds after 25 January. However, the LACCE data (Fig. 10) show that the same upwelling event coincided with the offshore movement of the Agulhas Current by 50 km and negative shear at the shelf edge, indicative of cyclonic flow offshore of the mooring transect. Roberts (2005) first noted the link between the cold ridge and the Agulhas Bight cyclonic eddy. More recently, a drifter study by Hancke et al. (this issue) showed that cyclonic flow in the

Agulhas Bight in summer promotes the offshore advection of coastal upwelling through the intensification of SW flow on the mid-shelf, inshore of the Agulhas Bight cyclone. They proposed that the absence of the cold ridge in winter is due to a lack of wind-driven coastal upwelling that feeds the cold ridge with cool and productive water.

To further investigate cold ridge formation, we present daily current vectors from three High Frequency (HF) Radar stations situated between Mossel Bay and Cape St Francis, overlaid on daily images of MUR SST for selected days in January and February 2019 (Fig. 12). These data reveal intermittent, but strong cyclonic flow in the Agulhas Bight from 21 January until the end of February when a train of meanders, with offshore dimensions of up to 50 km, progressed downstream in the Agulhas Current across altimeter track #198. Corresponding wind vectors and cross-shelf sections of the moored data at the CR transect (Fig. 13) confirm upwelling on the central shelf in late January and the formation of the cold ridge in February.

Coastal upwelling was first observed in satellite SST at the Tsitsikamma coast and further east at Port Alfred after strong easterly winds on 26/27 January. Satellite SST for 1 February (Fig. 12) shows two distinct cold-water plumes being advected westward from a coastal base, and a well-defined cyclonic eddy in the Agulhas Bight. The cold plume from the Port Alfred upwelling cell overlays the shelf break, inshore of the Agulhas Current. The second upwelling plume is advected offshore from the Tsitsikamma coast by the increased SW flow shoreward of the Agulhas Bight cyclone. This cool tongue remains visible and well defined at the surface along the 100 m isobath until 5 February despite a relaxation of upwelling winds after 2 February (Fig. 13a). The SST for 8 February shows extensive surface upwelling east of the CR transect after gale force easterlies on 6/7 February. Note the band of intense coastal upwelling inshore between Cape Seal and Cape St. Francis that anchors the upwelling to the coast. It is this cold-water base that Roberts (2005) and Hancke et al. (this issue) proposed to be the main source of cold water that sustains the cold ridge. The increased SW mid-shelf current, shoreward of the Agulhas Bight cyclone, steered the productive coastal water offshore, thus creating the classically curved cold ridge aligned with the mid-shelf bathymetry. This SW mid-shelf jet is evidently absent in the SST for 8 February (Fig. 12), when the cold ridge was not well defined.

Data from the UTR (Supplementary material S2) at Storms River Mouth confirm the onset of wind-driven upwelling on 26/27 January when the nearshore temperature decreased rapidly by 10 °C and remained <11 °C until 29 January while easterlies prevailed. Further west, at CR1, the upwelling signal was delayed by two days and less pronounced, with near-surface (23 m) temperatures decreasing by only 5 °C during the same period. At Storms River Mouth, temperature fluctuations >10 °C, over periods of 1–2 days corresponded to zonal

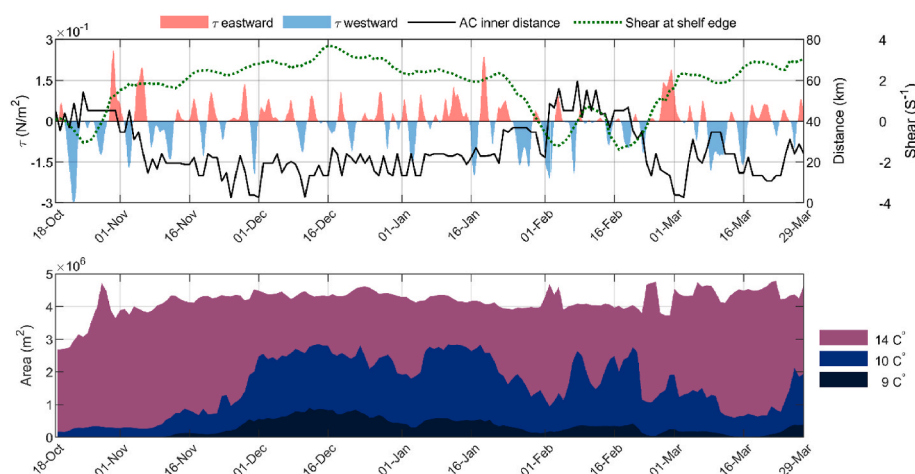


Fig. 10. (a) Left axis – Zonal wind stress (τ) averaged across the mooring transect. Positive (red) and negative (blue) wind stress values denote westerly and easterly winds respectively. Right axis (solid black line) – the distance of the shoreward edge of the Agulhas Current from shelf break as determined by the LACCE algorithm. Right axis (dotted green line) – daily AVISO-derived geostrophic current shear at the intersect of altimeter track #198 and the 200 m isobath. (b) The area associated with the 9 °C, 10 °C and 14 °C isotherms at the mooring transect over time.

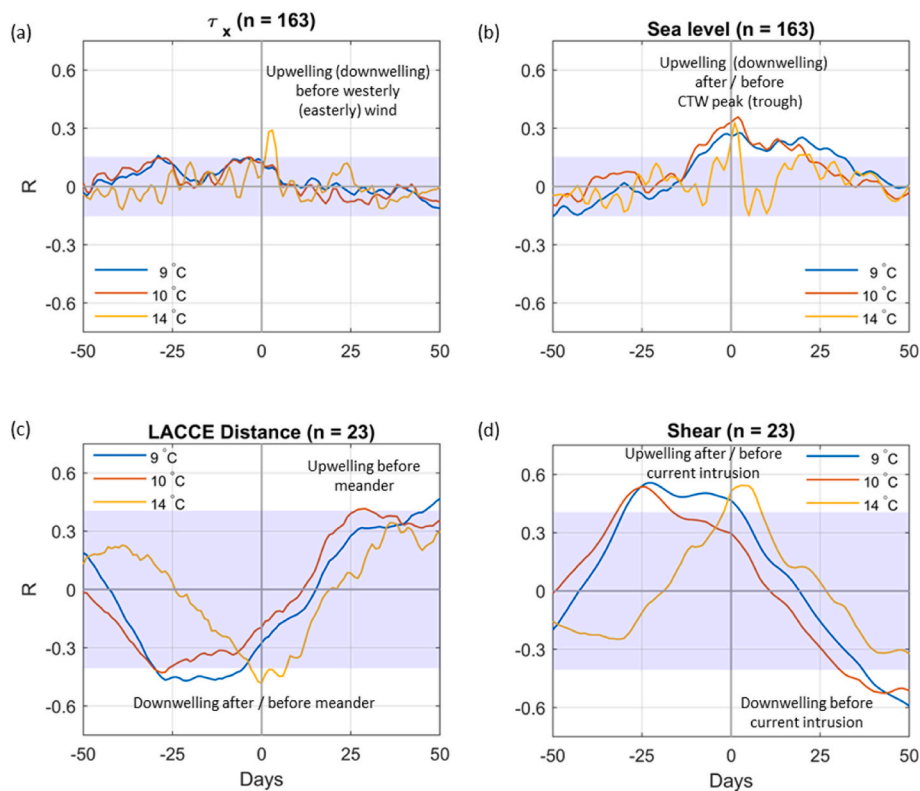


Fig. 11. Time-lag correlations of upwelling and downwelling at the CR mooring transect against (a) alongshore wind stress (τ_x), (b) coastal sea level at Mossel Bay, (c) the LACCE distance of the shoreward border of the Agulhas Current from the shelf edge and (d) AVISO derived current shear at the shelf edge. The 95% confidence interval based on $n = 163$ for (a) and (b) and $n = 23$ for (c) and (d) is shaded in grey. Blue, orange and yellow lines represents the area under the 9°C , 10°C and 14°C isotherms at the mooring transect respectively.

changes in the wind, but the near-surface temperature at the CR transect decreased more gradually and then remained $<12^\circ\text{C}$ at CR1 throughout February.

Cross-shelf sections of the temperature and velocity components at the mooring transect during the February upwelling event is shown in Fig. 13. On 30 January, three days after the start of upwelling at Storms River Mouth, a warm ($>20^\circ\text{C}$) surface layer covered a band of cool water ($<10^\circ\text{C}$), inshore of 100 m isobath. Isotherms in the nearshore tilted up towards the coast in response to offshore surface layer transport (not shown) during upwelling favourable conditions on 26–28 January. Sustained SW shelf flow between 31 January and 7 February corresponded to the presence of the Agulhas Bight cyclone seen in Fig. 12. The maximum SW shelf current occurred during periods of gale force easterly wind and upwelling on 1/2 February and again on 6/7 February. The subsequent formation of a cold-water dome ($<10^\circ\text{C}$), centred over the mid-shelf, is coincident with strong shear in the along-shelf flow. The doming is accentuated during the NE current reversal (8–10 February) that suppressed the 10°C isotherm in the inner shelf. The absence of strong westerly wind stress and large coastal sea level variation at the time suggests that the NE current shoreward of the 100 m isobath was not driven by a CTW, but rather by geostrophic flow around the cold ridge as proposed by Boyd et al. (1992).

The mean, depth-averaged temperature at the mooring transect in February remained $<12^\circ\text{C}$, despite NE current reversals on 8–10 February and 23–28 February, and extended periods without easterly wind (3–5 February; 8–13 February; 24–28 February).

4. Discussion and conclusion

Six months of in situ current and temperature measurements from a mooring array across the central Agulhas Bank captured the strengthening of seasonal stratification during the spring–summer deployment period that culminated in the formation of the cold ridge. The influx of the sub- 10°C water on the inner and mid-shelf (<100 m depth) in late spring confirms the main source of the cold bottom layer from further

east, as proposed by Largier and Swart (1987) and Lutjeharms (2006). Temperature records from a moored ADCP deployed on the continental slope (at a depth of 250 m) near altimeter track #198 (Krug et al., 2014) show that the greatest anomalies in seabed temperature along the shelf break occur during Natal Pulse events. The mooring transect in our study did not extend closer than 30 km from the shelf break and no Natal Pulse events were observed during the 6-month measurement period. However, continuous records of sub- 9°C water at the offshore mooring, during the encroachment of the Agulhas Current in December 2018 and in March 2019, show that the southern Agulhas Current in its ‘normal’ meandering mode made an important contribution to the cold basal layer through upwelling along the south-eastern shelf edge.

Advective forcing of the cold basal layer is further demonstrated through time-lag correlation analyses that show upwelling of South Indian Central water ($<9^\circ\text{C}$) and an increase in the thickness of the cold bottom layer ($<10^\circ\text{C}$) on the leading edge of meanders, and downwelling of these isotherms on the trailing edge of meanders, at significant lags periods of between 4 and 50 days. In contrast, surface cooling on the leading edge of meanders, and surface warming, associated with warm water plumes on the trailing edge of meanders, occurred at shorter lag times of between 0 and 6 days.

In the absence of in situ measurements offshore of the mooring transect, information on the behaviour and position of the Agulhas Current were derived from coarsely interpolated gridded altimetry. Krug et al. (2014) compared gridded, altimeter-derived geostrophic current velocities with ADCP measured currents near the shelf break and found that the gridded product underestimates SW surface flow at the shelf edge and was unable to adequately capture periods of NE current reversals during large meander events. Caution must therefore be exercised in interpreting the results from the time lag correlation analysis of advective forcing of upwelling. Nonetheless, these results support the theory of advective control of the thermocline on the central and eastern shelf (Swart and Largier 1987) and demonstrate the importance of the Agulhas Current in enhancing stratification from above and below.

ADCP measured currents confirm the predominantly barotropic

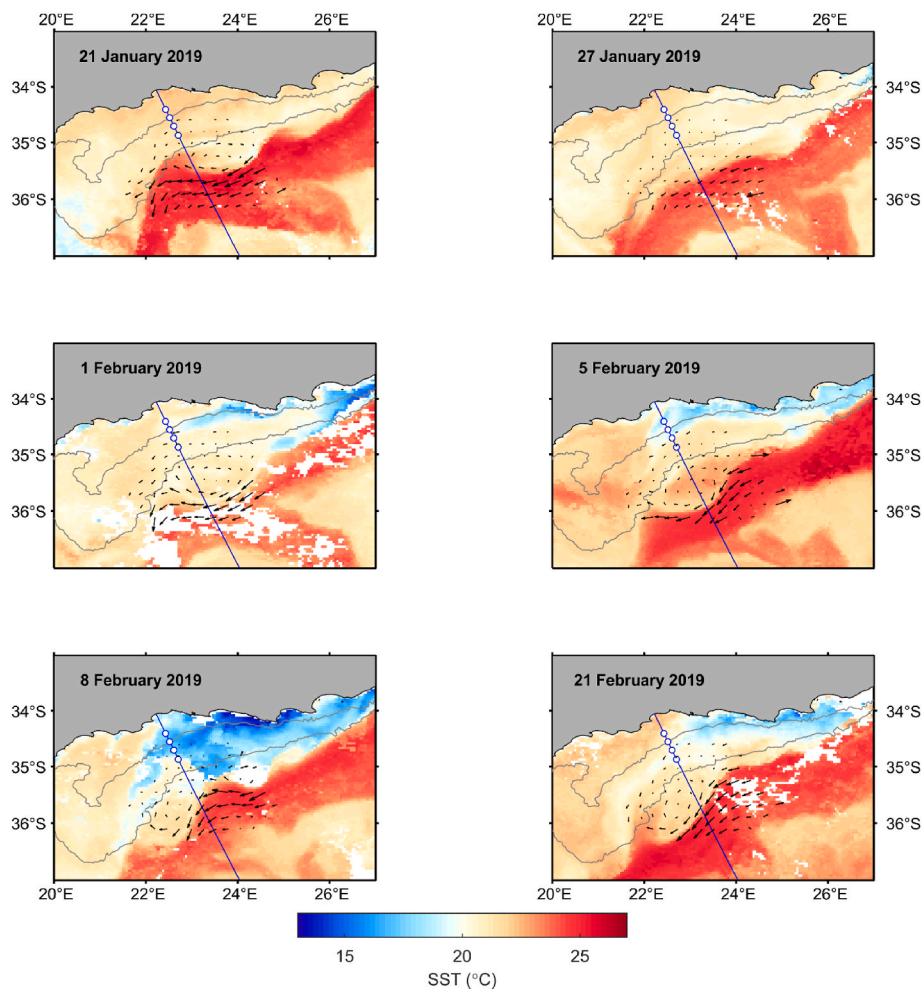


Fig. 12. Daily average current vectors from WERA HF Radar overlaid on MUR L4 SST over the Agulhas Bank for selected days in January and February 2019. The blue line is altimeter ground track #198 and blue circles show the CR mooring locations. The grey lines are the 100 m and 200 m isobaths.

nature of the along-shelf flow on the central and eastern Agulhas Bank as suggested by previous authors (Boyd et al., 1992; Krug et al., 2014; Schumann and Brink, 1990; Tilney et al., 1996). Currents on the central shelf were predominantly SW throughout the water column. Strong ($\sim 50 \text{ cm s}^{-1}$) barotropic pulses were significantly correlated with zonal wind stress and coastal sea level variation. NE reversals, accompanied by downwelling, were strongest and occurred most frequently on the inner shelf. Approximately 30% of barotropic reversals extended to the outer central shelf, resulting in a high level of coherence in the current structure across the central shelf. In contrast, currents on the Tsitsikamma coast were predominantly eastward. Strong ($\sim 80 \text{ cm s}^{-1}$) barotropic eastward pulses coincided with peak westerly wind and elevated coastal sea level. Currents at SRM were significantly correlated with the flow at the CR mooring transect at a lag of 6–8 hours, resulting in strong coherence and connectivity between the eastern and central shelf.

Synchronised along-shelf current reversals, attributed to coastal trapped waves (CTWs), have also been observed in surface drifter trajectories east of Cape Agulhas (Hancke et al. this issue). These transient sea level disturbances move anticlockwise around the South African coast and cause barotropic, current reversals with periods of 3–7 days during the passage of the peak of the wave (Goschen et al., 2012; Schumann and Brink, 1990). The majority of CTW on the South African south coast are remotely forced by wind events from the west (Bailey et al., 2022), but a condition of near resonance (Schumann and Brink, 1990) between the propagation speed of eastward moving weather systems and CTWs along this part of the shelf can result in the formation of large amplitude waves, and alongshore current reversals that are

sometimes perfectly timed with a change in wind direction (Attwood et al., 2002; Hancke et al., this issue). Jury and Brundrit (1992) showed an association between CTWs and upwelling cycles on the western Agulhas Bank, with enhanced upwelling/downwelling during the trough/peak of a CTW. Given the prevalence of large amplitude CTWs to occur along the wind-driven upwelling zone off the southern Cape coast, their role in regulating thermohaline processes and productivity on the shelf should be addressed in future research.

The emergence of the cold ridge in late January and its presence throughout February resulted from a combination of factors. (1) Seasonal stratification was already well established with sub-10 °C water present at 50 m depth on the inner and mid-shelf. (2) Strong and sustained easterly wind stress drove intense coastal upwelling east of Knysna. The divergence of the Agulhas Current from the coast at Port Alfred certainly also contributed to the persistent upwelling seen in SST images on the far eastern Agulhas Bank throughout February. Upwelling plumes from Port Alfred and the Tsitsikamma coast merged laterally and moved SW with the shelf circulation. (3) Intensification of SW flow on the mid-shelf, shoreward of cyclonic flow in the Agulhas Bight, resulted in accelerated advection of coastal upwelling and the formation of a classically shaped cold ridge. (4) Subsequent NE current reversals and downwelling near the coast accentuated the characteristic doming of isotherms over the mid-shelf that constitutes the cold ridge and resulted in intermittent cyclonic flow around the cold ridge as postulated by (Boyd et al., 1992). The absence of evidence of CTWs in the sealevel data at the time suggests that this mid-shelf cyclonic flow around the cold ridge was geostrophically driven.

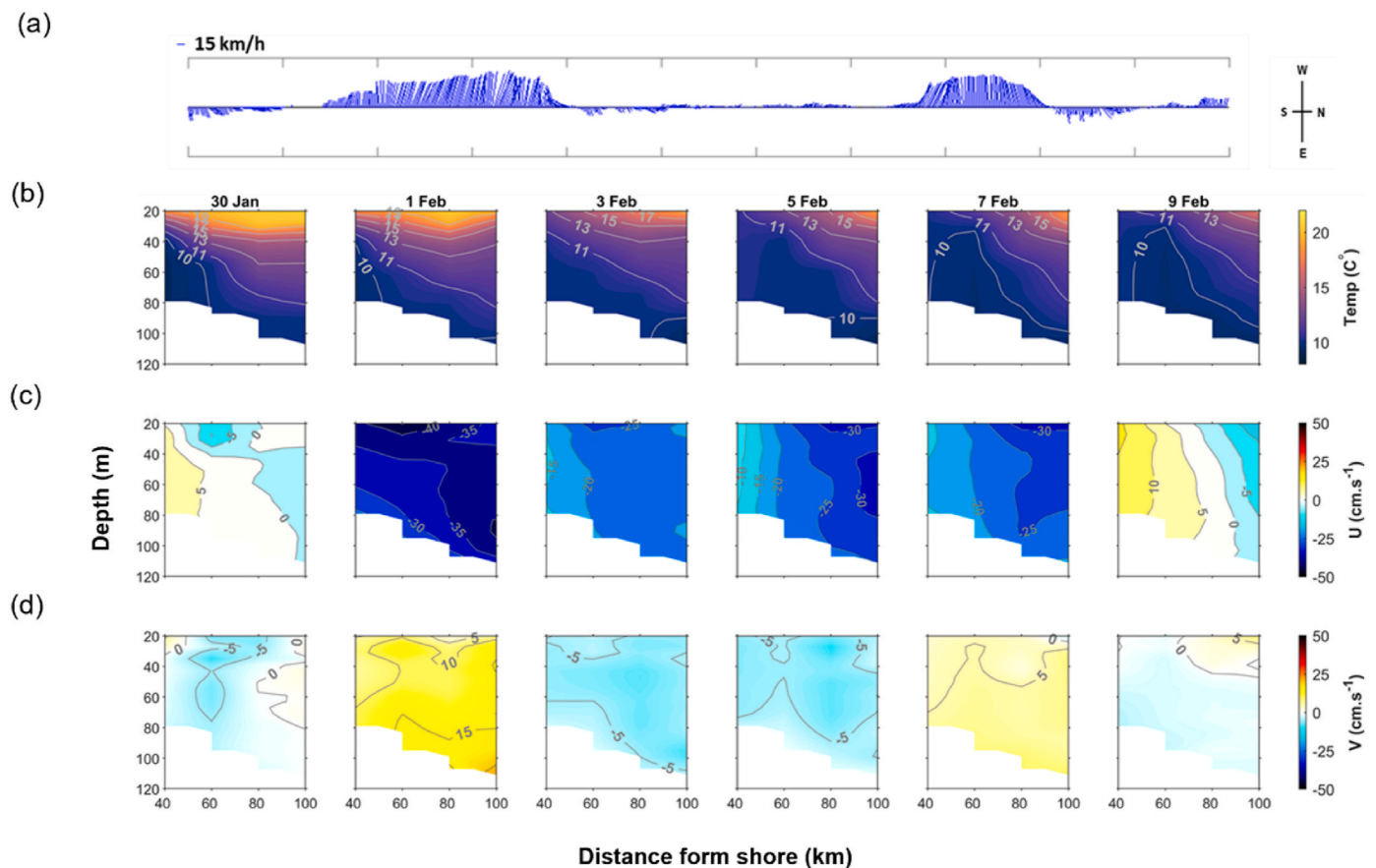


Fig. 13. Supporting data for the cold ridge formation case study in January and February 2019. (a) Hourly wind vectors at the mooring transect. Axes are rotated 90° clockwise so that upward and downward pointing vectors represent easterly (upwelling) and westerly (downwelling) winds respectively. Daily averaged cross-shelf sections of (b) temperature, (c) the along-shelf (u) current and (d) the cross-shelf (v) current at the mooring transect given at 2-day intervals. For the along-shelf current negative (blue) and positive (red) values denote south-westward and north-eastward flow respectively. For the cross-shelf current negative (blue) and positive (red) values denote south-eastward (offshore) and north-westward (onshore) flow respectively. The x-axis shows the distance from shore, with the CR moorings 1–4 located at 40, 60, 80 and 100 km respectively.

Future predictions for the Agulhas Bank show both an increase in the strength of the Agulhas Current and in upwelling-favourable wind stress associated with a shift in global wind patterns (Backeberg et al., 2012; Jury, 2020). This is in line with a regime shift to cooler temperatures observed on the Agulhas Bank in the late 1990's (Malan et al., 2019). However, Elipot and Beal (2018) suggest that intra-annual variability in the Agulhas Current outweighs long-term trends. With this in mind, long-term in situ monitoring of the Agulhas Current and the adjacent shelf environment is critical in understanding the complexities of the system and the impact of environmental change on resource management on the Agulhas Bank in the near future.

Author contribution statement

Lisa Hancke: Conceptualization, Methodology, Investigation, Formal Analysis, Writing - Original Draft, Review & Editing, Visualization. David Smeed: Analysis, Validation, Supervision, Writing - Review & Editing. Michael J. Roberts: Conceptualization, Supervision, Funding acquisition. Cristina Russo: Analysis, Writing - Original Draft, Review & Editing. Darren Rayner: Data Processing (Mooring Behaviour Model). Fatma Jebri: Writing - Review & Editing.

Declaration of competing interest

The authors declare the following financial interests/personal relationships which may be considered as potential competing interests: L. Hancke reports administrative support and travel were provided by

SOLSTICE-WIO. L. Hancke reports financial support was provided by South African Institute for Aquatic Biodiversity.

Data availability

Data will be made available on request.

Acknowledgements

This publication was produced with the financial support of the Global Challenges Research Fund (GCRF), United Kingdom, within the framework of the SOLSTICE-WIO project, under NERC grant NE/P021050/1. We thank the South African Institute for Aquatic Biodiversity (SAIAB) – ACEP PhD Bursary and the Nelson Mandela University (NMU) Post Graduate Scholarship (PGRS) for funding and support. This work is also part of the UK-SA Ocean Science and Marine Food Security Bilateral Research Chair funded by the NRF/DST Grant (98399) and the British Council grant (SARCII50326116102).

We acknowledge the following data sources: The South African Weather Service (SAWS) for data from the coastal weather stations.

- The South African Hydrographic Office (SANHO) for providing access and assistance with processing the tide gauge data.

- South Africa's Department of Forestry, Fisheries and Environment (DFFE) for access to the coastal underwater temperature recorder (UTR) data.

- Copernicus Climate Change Service (C3S) Climate Data Store (CDS) for the ERA5 hourly data on single levels from 1979 to present. Accessed

2020-11-23 at 10.24381/cds.adbb2d47.

- JPL MUR MEaSUREs Project. 2015. GHRSSST Level 4 MUR Global Foundation Sea Surface Temperature Analysis. Ver. 4.1. PO.DAAC, CA, USA. Dataset accessed 2020-06-25 at <https://doi.org/10.5067/GHGMR-4FJ04>.

- Actimar, CLS Southern Africa and Total Energies for access to the WERA HF Radar dataset.

Appendix A. Supplementary data

Supplementary data to this article can be found online at <https://doi.org/10.1016/j.dsr2.2023.105293>.

References

- Attwood, C.G., Allen, J., Claassen, P.J., 2002. Nearshore surface current patterns in the Tsitsikamma national park, South Africa. *S. Afr. J. Mar. Sci.* 24, 151–160. <https://doi.org/10.2989/025776102784528448>.
- Backeberg, B., Penven, P., Rouault, M., 2012. Impact of intensified Indian Ocean winds on mesoscale variability in the Agulhas system. *Nat. Clim. Change* 2, 608–612. <https://doi.org/10.1038/nclimate1587>.
- Bailey, D.F., Hermes, J., Penven, P., Bornman, T.G., Goschen, W., 2022. An investigation of sea level and circulation response during a coastal trapped wave event on the Eastern Agulhas Bank, South Africa. *Cont. Shelf Res.* 240. <https://doi.org/10.1016/j.csr.2022.104698>.
- Beckley, L.E., 1988. Spatial and temporal variability in sea temperature in Algoa Bay, South Africa. *S. Afr. J. Mar. Sci.* 84, 67–69.
- Boyd, A.J., Shillington, F.A., 1994. Physical forcing and circulation patterns on the Agulhas Bank. *South Afr. J. Sci.* 90, 114–122.
- Boyd, A.J., Taunton-Clark, J., Oberholster, G.P.J., 1992. Spatial features of the near-surface and midwater circulation patterns off western and southern South Africa and their role in the life histories of various commercially fished species. *S. Afr. J. Mar. Sci.* 12, 189–206. <https://doi.org/10.2989/02577619209504702>.
- Chang, N., 2008. Numerical Ocean Model Study of the Agulhas Bank and the Cool Ridge. Univ. Cape T. <https://doi.org/10.1016/j.renene.2008.06.018>.
- Chapman, P., Largier, J.L., 1989. On the origin of Agulhas Bank bottom water. *South Afr. J. Sci.* 85, 515–519.
- Elipot, S., Beal, L., 2018. Observed Agulhas Current sensitivity to interannual and long-term trend atmospheric forcings. *J. Clim.* 31. <https://doi.org/10.1175/JCLI-D-17-0597.1>.
- Goschen, W.S., Bornman, T.G., Deyzel, S.H.P., Schumann, E.H., 2015. Coastal upwelling on the far eastern Agulhas Bank associated with large meanders in the Agulhas Current. *Continent. Shelf Res.* 101, 34–46. <https://doi.org/10.1016/j.csr.2015.04.004>.
- Goschen, W.S., Schumann, E.H., 1994. An agulhas current intrusion into alga bay during august 1988. *S. Afr. J. Mar. Sci.* 14, 47–57. <https://doi.org/10.2989/025776194784286914>.
- Goschen, W.S., Schumann, E.H., 1988. Ocean current and temperature structures in alga bay and beyond in november 1986. *S. Afr. J. Mar. Sci.* 7, 101–116. <https://doi.org/10.2989/025776188784379198>.
- Goschen, W.S., Schumann, E.H., Bernard, K.S., Bailey, S.E., Deyzel, S.H.P., 2012. Upwelling and ocean structures off Algoa Bay and the south-east coast of South Africa. *Afr. J. Mar. Sci.* 34, 525–536. <https://doi.org/10.2989/1814232X.2012.749810>.
- Hancke, L., Roberts, M.J., Smeed, D., Jebri, F. This issue. Cold ridge formation mechanisms on the Agulhas Bank (South Africa) as revealed by satellite-tracked drifters. *Deep Sea Res. Part II Top. Stud. Oceanogr.* 208, 105245. <https://doi.org/10.1016/j.dsr2.2022.105245>.
- Helzel, T., Petersen, L., Mariette, V., Thomas, N., 2009. Accuracy and reliability of ocean current and wave monitoring with the coastal radar “WERA. In: OCEANS 2009-EUROPE, pp. 1–5. <https://doi.org/10.1109/OCEANSE.2009.5278303>.
- Hersbach, H., Bell, B., Berrisford, P., Biavati, G., Horányi, A., Muñoz Sabater, J., Nicolas, J., Peubey, C., Radu, R., Rozum, I., Schepers, D., Simmons, A., Soci, C., Dee, D., Thépaut, J.-N., 2019. ERA5 monthly averaged data on single levels from 1979 to present. Copernicus Climate Change Service (C3S) Climate Data Store (CDS). <https://doi.org/10.24381/cds.fl7050d7>. Accessed in 2019).
- Hutchings, L., Beckley, L.E., Griffiths, M.H., Roberts, M.J., Sundby, S., van der Lingen, C., 2002. Spawning on the edge: spawning grounds and nursery areas around the southern African coastline. *Mar. Freshw. Res.* 53, 307–318. <https://doi.org/10.1071/MF01147>.
- Jacobs, Z., Roberts, M., Jebri, F., Srokosz, M., Kelly, S., Sauer, W., Bruggeman, J., Popova, E. This issue. Drivers of productivity on the Agulhas Bank and the importance for marine ecosystems. *Deep Sea Res. Part II Top. Stud. Oceanogr.* 199, 105080. <https://doi.org/10.1016/j.dsr2.2022.105080>.
- Jury, M., 2020. Marine climate change over the eastern Agulhas Bank of South Africa. *Ocean Sci.* 16, 1529–1544. <https://doi.org/10.5194/os-16-1529-2020>.
- Jury, M.R., 1994. A review of the meteorology of the eastern Agulhas Bank. *South Afr. J. Sci.* 90, 109–113.
- Jury, M.R., Brundrit, G.B., 1992. Temporal organization of upwelling in the southern Benguela ecosystem by resonant coastal trapped waves in the ocean and atmosphere. *S. Afr. J. Mar. Sci.* 12, 219–224. <https://doi.org/10.2989/02577619209504704>.
- Kara, A.B., Wallcraft, A.J., Metzger, E.J., Hurlburt, H.E., Fairall, C.W., 2007. Wind stress drag coefficient over the global ocean. *J. Clim.* 20, 5856–5864. <https://doi.org/10.1175/2007JCLI1825.1>.
- Krug, M., Tournadre, J., Dufois, F., 2014. Interactions between the agulhas current and the eastern margin of the Agulhas Bank. *Continent. Shelf Res.* 81, 67–79. <https://doi.org/10.1016/j.csr.2014.02.020>.
- Largier, J.L., Chapman, P., Peterson, W.T., Swart, V.P., 1992. The western Agulhas Bank: circulation, stratification and ecology. *S. Afr. J. Mar. Sci.* 12, 319–339. <https://doi.org/10.2989/02577619209504709>.
- Largier, J.L., Swart, V.P., 1987. East-west variation in thermocline breakdown on the Agulhas bank. *S. Afr. J. Mar. Sci.* 5, 263–272. <https://doi.org/10.2989/025776187784522252>.
- Leber, G.M., Beal, L.M., 2015. Local water mass modifications by a solitary meander in the Agulhas Current. *J. Geophys. Res. Ocean.* 120, 4503–4515. <https://doi.org/10.1038/175238c0>.
- Leber, G.M., Beal, L.M., Elipot, S., 2016. Wind and current forcing combine to drive strong upwelling in the agulhas current. *J. Phys. Oceanogr.* 47, 123–134. <https://doi.org/10.1175/jpo-d-16-0079.1>.
- Lilly, J.M., 2021. jLab: A data analysis package for Matlab 1 (7.1). <https://doi.org/10.5281/zenodo.4547006>. <http://www.jmlilly.net/software>.
- Lutjeharms, J.R.E., 2006. *The Agulhas Current*. Springer Berlin Heidelberg.
- Lutjeharms, J.R.E., 1981. Features of the southern Agulhas Current circulation from satellite remote sensing. *South Afr. J. Sci.* 77, 231–236.
- Lutjeharms, J.R.E., Catzel, R., Valentine, H.R., 1989. Eddies and other boundary phenomena of the Agulhas Current. *Continent. Shelf Res.* 9, 597–616. [https://doi.org/10.1016/0278-4343\(89\)90032-0](https://doi.org/10.1016/0278-4343(89)90032-0).
- Lutjeharms, J.R.E., Cooper, J., 1996. Interbasin leakage through Agulhas current filaments. *Deep-Sea Res. Part I Oceanogr. Res. Pap.* 43, 213–238. [https://doi.org/10.1016/0967-0637\(96\)00002-7](https://doi.org/10.1016/0967-0637(96)00002-7).
- Lutjeharms, J.R.E., Cooper, J., Roberts, M., 2000. Upwelling at the inshore edge of the agulhas current. *Continent. Shelf Res.* 20, 737–761. [https://doi.org/10.1016/S0278-4343\(99\)00092-8](https://doi.org/10.1016/S0278-4343(99)00092-8).
- Lutjeharms, J.R.E., Durgadoo, J.V., Anson, L.J., 2007. Surface drift at the western edge of the Agulhas Bank. *South Afr. J. Sci.* 103, 63–67.
- Lutjeharms, J.R.E., Meyer, A.A., Anson, L.J., Eagle, G.A., Orren, M.J., 1996. The nutrient characteristics of the Agulhas bank. *S. Afr. J. Mar. Sci.* 17, 253–274. <https://doi.org/10.2989/025776196784158464>.
- Lutjeharms, J.R.E., Penven, P., Roy, C., 2003. Modelling the shear edge eddies of the southern Agulhas Current. *Continent. Shelf Res.* 23, 1099–1115. [https://doi.org/10.1016/S0278-4343\(03\)00106-7](https://doi.org/10.1016/S0278-4343(03)00106-7).
- Malan, N., Backeberg, B., Biastoch, A., Durgadoo, J.V., Samuelsen, A., Reason, C., Hermes, J., 2018. Agulhas current meanders facilitate shelf-slope exchange on the eastern Agulhas Bank. *J. Geophys. Res. Ocean.* 123, 4762–4778. <https://doi.org/10.1029/2017JC013602>.
- Malan, N., Durgadoo, J.V., Biastoch, A., Reason, C., Hermes, J., 2019. Multidecadal wind variability drives temperature shifts on the Agulhas Bank. *J. Geophys. Res. Ocean.* 124, 3021–3035. <https://doi.org/10.1029/2018JC014614>.
- Mazwane, S.L., Poulton, A.J., Hickman, A.E., Jebri, F., Jacobs, Z., Roberts, M., Noyon, M. This issue. Spatial and temporal variability of net primary production on the Agulhas Bank, 1998–2018. *Deep sea res. Part II top. Stud. Oceanogr.* 199, 105079. <https://doi.org/https://doi.org/10.1016/j.dsr2.2022.105079>.
- Pivan, X., Krug, M., Herbet, S., 2016. Observations of the vertical and temporal evolution of a natal pulse along the eastern Agulhas Bank. *J. Geophys. Res. Ocean.* 1–14. <https://doi.org/10.1002/2015JC011486>.
- Probyn, T.A., Mitchell-Innes, B.A., Brown, P.C., Hutchings, L., Carter, R.A., 1994. A review of primary production and related processes on the Agulhas Bank. *South Afr. J. Sci.* 90, 166–173.
- Rio, M.-H., Mulet, S., Picot, N., 2014. Beyond GOCE for the ocean circulation estimate: synergetic use of altimetry, gravimetry, and in situ data provides new insight into geostrophic and Ekman currents. *Geophys. Res. Lett.* 41, 8918–8925. <https://doi.org/10.1002/2014GL061773>.
- Roberts, M.J., 2005. Chokka squid (*Loligo vulgaris reynaudii*) abundance linked to changes in South Africa’s Agulhas Bank ecosystem during spawning and early life cycle. *ICES J. Mar. Sci.* 62, 33–55. <https://doi.org/10.1016/j.icesjms.2004.10.002>.
- Rouault, M., Penven, P., 2011. New perspectives on Natal Pulses from satellite observations. *J. Geophys. Res.* 116, C07013. <https://doi.org/10.1029/2010JC006866>.
- Russo, C.S., Lamont, T., Krug, M., 2021. Spatial and temporal variability of the Agulhas Retroflection: observations from a new objective detection method. *Remote Sens. Environ.* 253, 112239. <https://doi.org/10.1016/j.rse.2020.112239>.
- Russo, C.S., Lamont, T., Tutt, G.C.O., van den Berg, M.A., Barlow, R.G., 2019. Hydrography of a shelf ecosystem inshore of a major Western Boundary Current. *Estuar. Coast Shelf Sci.* 228, 106363. <https://doi.org/10.1016/j.ecss.2019.106363>.
- Schumann, E., Brink, K., 1990. Coastal-trapped waves off the coast of South Africa: generation, propagation and current structures. *J. Phys. Oceanogr.* 20, 1206–1218. [https://doi.org/10.1175/1520-0485\(1990\)020<1206:TWOTC>2.0.CO;2](https://doi.org/10.1175/1520-0485(1990)020<1206:TWOTC>2.0.CO;2).
- Schumann, E.H., 1999. Wind-driven mixed layer and coastal upwelling processes off the south coast of South Africa. *J. Mar. Res.* 57, 671–691. <https://doi.org/10.1357/002224099321549639>.
- Schumann, E.H., Perrins, L.A., Hunter, I.T., 1982. Upwelling along the South coast of the Cape province, South Africa. *South Afr. J. Sci.* 78, 238–242.
- Schumann, E.H., van Heerden, I.L., 1988. Observations of agulhas current frontal features south of Africa, october 1983. *Deep-Sea Res., Part A* 35, 1355–1362. [https://doi.org/10.1016/0198-0149\(88\)90087-8](https://doi.org/10.1016/0198-0149(88)90087-8).
- Shannon, L., 1985. The Benguela ecosystem. I: evolution of the Benguela physical features and processes. *Oceanogr. Mar. Biol.* 23, 105–182.

- Swart, V.P., Largier, J.L., 1987. Thermal structure of Agulhas bank water. *S. Afr. J. Mar. Sci.* 5, 243–252. <https://doi.org/10.2989/025776187784522153>.
- Tilney, R., Nelson, G., Radloff, S., Buxton, C., 1996. Ichthyoplankton distribution and dispersal in the Tsitsikamma National Park marine reserve , South Africa. *S. Afr. J. Mar. Sci.* 17, 1–14.
- Verheye, H.M., Hutchings, L., Huggett, J.A., Carter, R.A., 1994. Community structure, distribution and trophic ecology of zooplankton on the agulhas bank with special reference to copepods. *South Afr. J. Sci.* 90, 154–165.
- Walker, N.D., 1986. Satellite observations of the Agulhas Current and episodic upwelling south of Africa. *Deep. Res. Part A* 33, 1083–1106.